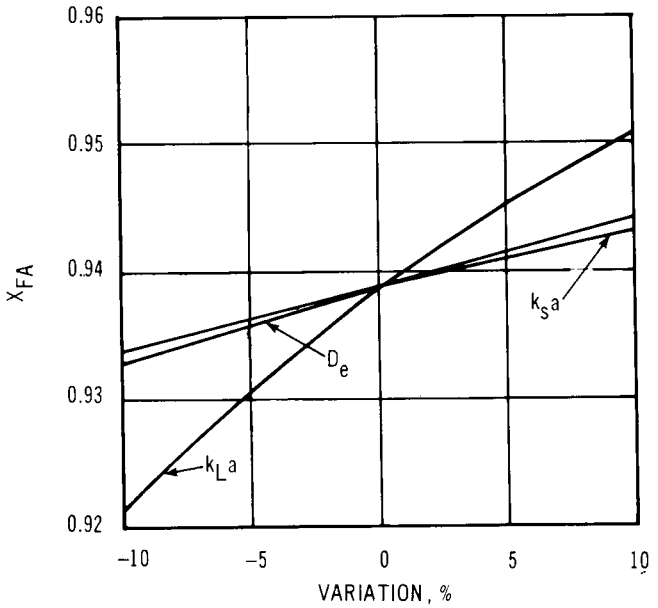

Fig. 11. Sensitivity of conversion to rate coefficients (F_L = 0.9 and F_g = 4.0 cm³/s, d_p = 0.291 cm, t = 240°C, p = 40 atm).

The quantitative effect on the conversion of the three local transport processes is shown in Figure 11. Here the usual values of k_La, k_sa and D_e are used in the computations, except one of them is varied by the amount indicated on the abscissa. The ordinate values show the corresponding change in conversion. The dominating effect of k_La is again evident. Since k_La is dependent upon the somewhat uncertain estimates of diffusivities, it is not unlikely that the predicted values for this rate coefficient are in error. The calculations for the conversion shown in Figure 11 for a 10% lower value of k_La, for one particle size and set of flow rates, were repeated for other conditions using the plug-flow model. The results are indicated by the dotted lines in Figures 6 and 7. Comparison with the solid lines shows that a 10% error in k_La has a greater effect than inclusion of axial dispersion in the model. Also a 10% error in k_La is enough to account for the difference between predicted and experimental conversions. It should be noted that the restriction in our work to uniform liquid distribution poses important limitations in using the results for scale-up. Nonuniform distribution is normal in large-diameter reactors, and this can affect performance significantly, particularly at high conversions. Also scale-up may lead to linear liquid velocities much different than those employed in our work. At widely different velocities the flow regime in the reactor may be different (Weekman and Myers, 1964) with probably different mass transfer coefficients. For example, axial dispersion and reduction in effective mass transfer area (due to inadequate wetting of the particles) could be much more important at very low liquid velocities.

ACKNOWLEDGMENT

The financial assistance of the Water Resources Center, University of California, Grant W-392, is gratefully acknowledged. The ZnO·CuO catalyst was supplied by the Chemetron Corporation.

NOTATION

(See Part I).

LITERATURE CITED

(See Part I).

Manuscript received December 2, 1974; revision received February 3 and accepted February 14, 1975.

Stresses and Friction Forces in Moving Packed Beds

A model to determine stresses and friction forces in moving packed beds with interstitial fluid flow has been developed. The scaling parameters are determined from the governing equations. A plane and an axisymmetric bed geometry are studied and the wall stress calculated under uniform one-dimensional axial flow conditions. The effect of added transverse flow (for example, due to a screen in the wall) is investigated. The present model is an improvement over earlier, one-dimensional models with capability to include in the stress analysis varying pressure gradients in all directions which may exist in practical moving bed systems.

GERSHON GROSSMAN

Faculty of Mechanical Engineering
Technion—Israel Institute of Technology
Haifa, Israel

SCOPE

Packed beds of granular solids flowing through a column as a consolidated plug have had wide application in chemical and physical processes involving solid-fluid interactions. While most such systems have relied on gravity-induced motion of the bed (with co-flow or counterflow of the contacting fluid), there has been growing interest in recent years in utilizing the fluid drag of the co-flow as a driving force for the bed, which provides for better control and higher bed velocities. The moving bed idea has been applied to the design of several continuous and semi-continuous solid-liquid contactors for processes such as crystal washing and ion exchange (Aerhart et al., 1956; Hancher and Jury, 1959; Shwartz and Probstein, 1969; Gold et al., 1971, 1973).

In many of the moving bed systems, especially in those with fluid counterflow, difficulties have been encountered

in achieving a stable, steady motion of the bed due to the high friction forces exerted on it by the column walls. Several studies have been made trying to analyze and determine the stresses in a moving bed. Delaplaine (1956) investigated the forces acting in granular solids flowing downward by gravity. His work was extended by Hancher and Jury (1959) and later by Brandt and Johnson (1963) to include stresses induced by fluid flow through the bed. These studies were all based on a one-dimensional flow model, which assumed, following Janssen (1895), a constant ratio of the normal stress at the wall to the average axial stress at each cross section of the column. Experiments with one dimensional flow, concurrent and countercurrent to the bed motion, have shown satisfactory agreement with this model in some cases and not so good in others (Brandt and Johnson, 1963). However, the assumption of constant ratio between wall and average axial stress was shown to be inaccurate in most cases (Brandt and Johnson). Also, the one-dimensional model is too simplified for describing actual systems involving columns with screens in the wall for fluid inlets and outlets (Gold et al., 1971, 1973), as it does not take into account the effect of the transverse flow toward the screen and the additional stresses associated with it. It appears that a more rigorous, two-dimensional analysis is in order.

The stress distribution in a bed of granular solids depends on the external load as well as on two properties: the friction coefficient between the particles and their cohesiveness (Jenike and Johanson, 1970; Sokolovski, 1965). These properties determine the planes of deformation, also known as *slip lines,* along which the particles move relative to each other when the stresses in the bed are sufficiently high. Treating the bed as a continuum, there exist in the general three-dimensional case three normal and three tangential unknown stresses at each point to be determined from three equilibrium equations and additional information on the behavior of the granular medium (Sokolovski, 1965). A detailed point by point analysis is, therefore, often very difficult. A great deal of work in this area has been done by Jenike and Johanson (1959, 1964, 1969, 1970) who applied the basic soil mechanics equations to the flow of granular solids in hoppers and bins under the influence of gravity.

The purpose of the present study has been to develop a detailed two-dimensional model for a packed bed moving in a column with interstitial fluid flow. This model enables to determine the stresses induced in the bed by the fluid and the wall friction resulting therefrom and may provide the basis for design of continuous solid-liquid contactors and other moving bed systems.

CONCLUSIONS AND SIGNIFICANCE

An improved two-dimensional model based on continuum properties of a granular medium has been developed to determine stresses and friction forces in moving packed beds. The detailed stress distribution in the bed has been studied (Figure 3) with a particular emphasis on the shear and friction forces between its particles and the column walls. The scaling parameters were determined from the governing equations indicating a direct relation of all stresses to the effective pressure difference ΔP_e across the bed divided by its aspect ratio L/D. An integral method of solution has been applied yielding results very close to those of an exact solution by the method of characteristics.

A plane (two-dimensional) and an axisymmetrical bed geometry were studied. Shear stresses and friction forces at the wall were calculated under uniform one-dimensional axial flow conditions. The analysis shows in both cases a practically linear growth of the shear stress at the wall with the axial length y (scaled with the column width) as shown in Figures 4 and 5. An upper limit on the length of the moving bed is set by the fact that wall friction increases faster with y than the driving force [Equations (31) and (40)]. The shear and friction increase directly with the wall friction coefficient μ_w and decrease with the internal friction coefficient μ.

The effect of added transverse flow (due, for example, to a screen in the wall) has been studied on a two-dimensional column with a flow-permeable wall. With bed properties and axial pressure difference ΔP being fixed, the shear stress and friction at the wall increase with the added transverse flow (expressed by γ) as shown in Figure 7, due to the associated pressure gradient from center to wall which increases the normal force on the wall.

The model developed in this study is based on a rigorous, point by point continuum approach to the behavior of a granular medium under stress and may be considered an improvement over earlier, more crude one-dimensional models (Janssen, 1895; Delaplaine, 1956; Hancher and Jury, 1959). Its significance lies in the fact that both axial and transverse pressure gradients, varying from point to point in the bed may be taken into account in the stress analysis and their effect on wall friction evaluated. A direct example is the solution for the stresses and friction caused by the transverse flow in the vicinity of a screen treated in the last section. The model may be applied in a similar manner to other important moving bed systems with more complex flow conditions and geometries.

MODEL AND EQUATIONS

Figure 1a describes a packed bed of granular solids of length L moving downward through a column. The bed may be either two-dimensional of width $2D$, or axisymmetrical of radius D, with X and Y representing the transverse and axial coordinates in a cartesian or in a cylindrical coordinate system, respectively. A pressure difference ΔP applied between the ends of the bed causes liquid flow through it. In the case of concurrent flow shown in Figure 1a, both gravity and fluid drag provide the driving force for the motion. With a reverse pressure difference counter flow takes place in which case the driving force would be gravity alone. The bed is composed of rigid, incompressible, and cohesionless particles with internal friction coefficient μ and friction coefficient with the wall μ_w. The permeability K and porosity ϵ are assumed to be uniform throughout the bed.

Figure 2a shows a small element of the two-dimensional bed with the stresses σ_{xx}, σ_{yy}, and $\tau_{xy} = \tau_{yx}$ acting on it. In the axisymmetrical element (Figure 2b) an additional circumferential stress $\sigma_{\theta\theta}$ is present, which may be expressed in terms of the other stresses by the Haar-Von Karman (1909) hypothesis. Other forces acting on the elements are the fluid drag manifested by a pressure gradient and the net gravity force (weight minus buoyancy). A force balance for the elements yields two equilibrium equations:

$$\frac{\partial \sigma_{xx}}{\partial X} + \frac{m}{X}(\sigma_{xx} - \sigma_{\theta\theta}) + \frac{\partial \tau_{yx}}{\partial Y} = -\frac{\partial P}{\partial X} \qquad (1)$$

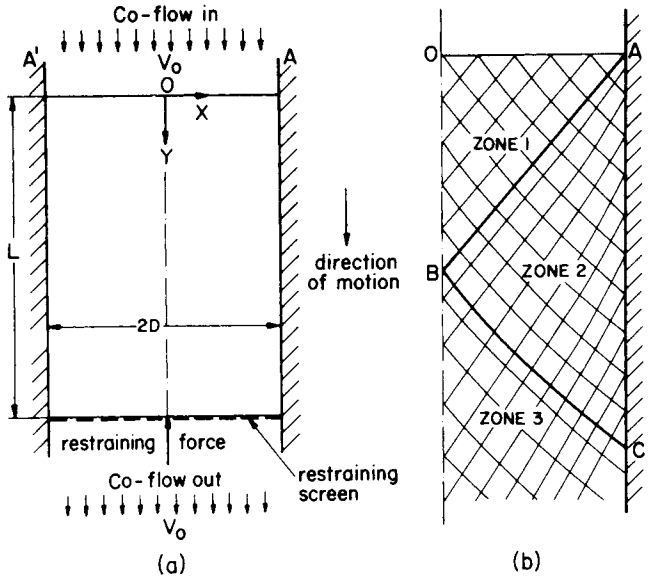

Fig. 1. Two-dimensional column with one-dimensional flow. Characteristics are plotted for $\mu = 0.20$ and $\mu_w = 0.10$.

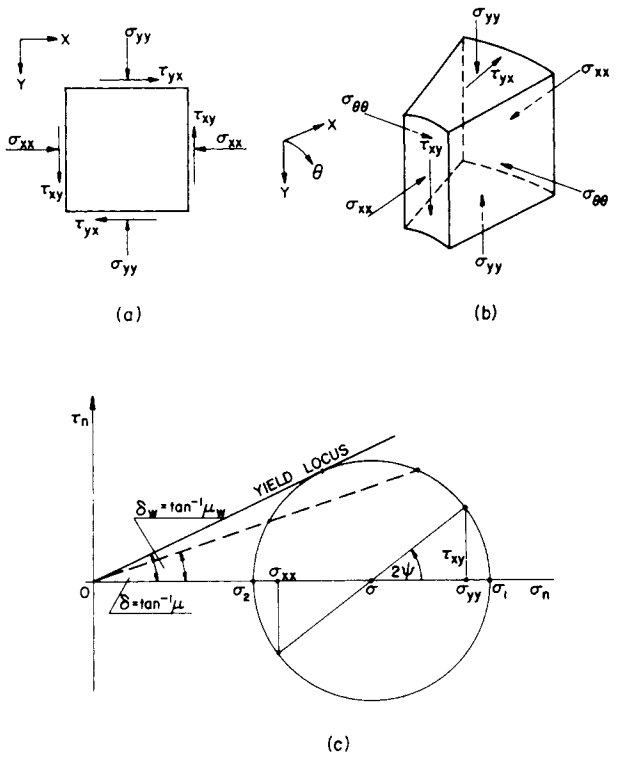

Fig. 2. Stresses in a moving bed: (a) two-dimensional element; (b) axisymmetrical element; (c) Mohr's circle with stress relations for granular medium in limiting equilibrium.

$$\frac{\partial \tau_{xy}}{\partial X} + \frac{m}{X}\tau_{xy} + \frac{\partial \sigma_{yy}}{\partial Y} = -\frac{\partial P}{\partial Y} + (\rho_s - \rho_f)(1-\epsilon)g \tag{2}$$

where ρ_s and ρ_f are the densities of the solid particles and the fluid, respectively, $m = 0$ for two-dimensional and $m = 1$ for axisymmetrical geometry.

An additional equation for the three unknown stresses is based on the properties of the medium, as is the case, for example, in a stress analysis of an elastic solid. The granular medium is simpler to analyze since no stress-strain relations have to be written and the deformation mechanism may be described in terms of a pure stress relation known as the yield function (Jenike and Shield, 1959). While the individual particles are rigid, the bed as a whole tends to deform slightly under the applied load as it conforms to minor imperfections in the cylindrical shape of the column or changes its compaction locally due to the constantly varying stresses. Deformation of the bed under stress occurs through relative motion and reorientation of the particles, which take place when the stresses present overcome the forces of internal friction. Mohr's circle describing the relative magnitude of normal and shear stresses (Figure 2c) shows that at some angle to the principal axes there is a plane where the ratio of shear to normal stress is a maximum. When this ratio becomes higher than μ, motion of the particles takes place along this plane. It follows that when the bed is in limiting equilibrium Mohr's circles for all points must be tangent to the so-called *yield locus* (Jenike and Shield, 1959) as shown in Figure 2c and the following stress relation is obtained:

$$\frac{(\sigma_{yy} - \sigma_{xx})^2 + 4\tau^2_{xy}}{(\sigma_{yy} - \sigma_{xx})^2} = \frac{\mu^2}{1+\mu^2} \tag{3}$$

It should be noted that Equation (3) is quadratic and has two roots defining two limiting equilibrium stress fields which may develop under different conditions. Using soil mechanics terminology, they are known as the active and passive fields, the former caused directly by the load with the large normal stress in the axial direction and the latter caused by a reaction at the wall with the large stress perpendicular to the wall. These two fields enclose a range of elastic fields which develop when the bed is not in limiting equilibrium, for example, when there is no tendency for it to deform or during certain transitions from active to passive stress field due to a change in the load. Under the conditions of the problems discussed in the present study, the direction of the load is fixed leading to constantly increasing normal stresses in the axial direction. Also, it is assumed that any imperfection in the cylindrical shape of the column is a divergence (which is, in fact, an important requirement in the actual design of moving bed systems), and therefore the entire bed is in active limiting equilibrium as described by $\sigma_{yy} > \sigma_{xx}$ in Equation (3).

The equations may be written in a dimensionless form, normalizing all lengths with respect to the column half width D, and all the stresses with respect to the effective pressure difference ΔP_e divided by the aspect ratio of the bed L/D. Here

$$\Delta P_e = \Delta P + (\rho_s - \rho_f)(1-\epsilon)gL \tag{4}$$

The dimensionless variables are

$$\sigma_x = \frac{\sigma_{xx}}{(D/L)\Delta P_e}; \quad \sigma_y = \frac{\sigma_{yy}}{(D/L)\Delta P_e}; \quad \sigma_\theta = \frac{\sigma_{\theta\theta}}{(D/L)\Delta P_e}$$

$$\tau = \frac{\tau_{xy}}{(D/L)\Delta P_e}; \quad p = \frac{P}{(D/L)\Delta P_e} \tag{5}$$

$$x = \frac{X}{D}; \qquad y = \frac{Y}{D}$$

and the equations become

$$\frac{\partial \sigma_x}{\partial x} + \frac{m}{x}(\sigma_x - \sigma_\theta) + \frac{\partial \tau}{\partial y} = -\frac{\partial p}{\partial x} \tag{6}$$

$$\frac{\partial \tau}{\partial x} + m\frac{\tau}{x} + \frac{\partial \sigma_y}{\partial y} = -\frac{\partial p}{\partial y} + \frac{(\rho_s - \rho_f)(1-\epsilon)gL}{\Delta P_e} \tag{7}$$

$$\frac{(\sigma_y - \sigma_x) + 4\tau^2}{(\sigma_y + \sigma_x)^2} = \frac{\mu^2}{1 + \mu^2} \tag{8}$$

with the boundary conditions:

$$\text{at} \quad y = 0 \quad \sigma_x = \sigma_y = \tau = 0; \quad \text{at} \quad x = 0 \quad \tau = 0$$
$$\text{at} \quad x = 1 \quad \tau = \mu_w \sigma_x \tag{9}$$

TWO-DIMENSIONAL COLUMN WITH ONE-DIMENSIONAL FLOW

Consider again the two-dimensional column of Figure 1a. A rigid restraining screen of negligible weight and no resistance to flow is added at the downstream end of the bed to prevent its unpacking by fluidization. An upward restraining force is applied to the bed through the screen to balance the driving force in excess of the amount required to move the bed at constant velocity against the wall friction. This model may describe a typical continuous moving bed system such as a crystal washer or an ion exchange column (Schwartz and Probstein 1969; Gold et al. 1971), with the restraining screen representing a flow-permeable device constantly removing particles off the downstream end of the bed, and where the incoming flow is a slurry containing particles constantly rebuilding the bed at the upstream end so that a steady state is maintained. The column has no side screens and its walls are impermeable to flow. With the pressure difference ΔP applied between the ends of the bed, this results in a one-dimensional Darcy flow at uniform velocity v_0 through the column, associated with a uniform pressure gradient parallel to the y direction:

$$\frac{\partial P}{\partial X} = 0; \quad \frac{\partial P}{\partial Y} = -\frac{\Delta P}{L} = -\frac{\eta}{K} v_0 \tag{10}$$

and the dimensionless equilibrium equations for two-dimensional geometry (6) and (7) become

$$\frac{\partial \sigma_x}{\partial x} + \frac{\partial \tau}{\partial y} = 0 \tag{11}$$

$$\frac{\partial \tau}{\partial x} + \frac{\partial \sigma_y}{\partial y} = 1 \tag{12}$$

Solution by the Method of Characteristics

Equations (11), (12), and (8) are hyperbolic and may be transformed into another form convenient to solve by the method of characteristics. The transformation and method of solution, including the numerical procedure, have been described in detail by Sokolovski (1965). First, the three unknown stresses are expressed in terms of two new variables: σ—the mean of the two normal stresses, and ψ—the angle with the principal axes (Figure 2c). Let

$$\left.\begin{aligned} &\sigma_x = \sigma(1 - \sin\delta \cos 2\psi); \quad \sigma_y = \sigma(1 + \sin\delta \cos 2\psi) \\ &\tau = \sigma \sin\delta \sin 2\psi \end{aligned}\right\} \tag{13}$$

The condition for limiting equilibrium, expressed by the yield function (8) is automatically satisfied. Substituting (13) in (11) and (12) and taking an appropriate linear combination of the resulting equations, the transformed set is obtained with the first and second characteristic directions given by

$$\left(\frac{dy}{dx}\right)_2 = \tan\left[-\psi \pm \left(\frac{\pi}{4} + \frac{\delta}{2}\right)\right] \tag{14}$$

The characteristic directions are inclined at angles $\pm (\pi/4 - \delta/2)$ to the major principal axis, and are also slip lines (Sokolovski, 1965). The equilibrium equations are replaced by

$$d\sigma \pm 2\sigma \tan\delta d\psi = dy \mp \tan\delta dx \tag{15}$$

with the upper and lower sign taken along the first and second characteristic, respectively. The boundary conditions (9) become

$$\left.\begin{aligned} &\text{at} \quad y = 0 \quad \sigma = 0; \quad \text{at} \quad x = 0 \quad \psi = 0 \quad \sigma = \frac{y}{1 + \sin\delta} \\ &\text{at} \quad x = 1 \quad \psi = \psi_w = \frac{1}{2}\left[\sin^{-1}\left(\frac{\sin\delta_w}{\sin\delta}\right) - \delta_w\right] \end{aligned}\right\} \tag{16}$$

Figure 1b shows a typical plot of the characteristics in the right half of the column.* Three different zones are distinguishable. In zone 1 (AOB) $\psi = 0$ everywhere, the shear stresses are zero and the effect of wall friction is unnoticed. The ratio of σ_x to σ_y is constant and the characteristics are straight lines inclined at $\pm (\pi/4 - \delta/2)$ to the y axis. In zone 2 (ABC) the wall effect begins to develop with y. The characteristics bend toward the wall to make an angle $\psi_w \pm (\pi/4 - \delta/2)$ with it and shear stresses appear. In zone 3 (below the line BC), the wall effect has reached the center of the column. The increase in the effect of wall friction with y is further illustrated in Figure 3, which shows stress profiles at various cross sections of the bed calculated from values of σ and ψ.

The shear stress and total friction force at the wall are shown in Figure 4 as functions of y for various values of μ and μ_w. The dimensionless shear stress T varies almost linearly with y, increases with wall friction coefficient μ_w, and decreases with μ. The latter decrease is explained by the fact the higher internal coefficient causes less of the axial stress to be transmitted sideways as a force normal to the wall. The dimensionless total friction force f is

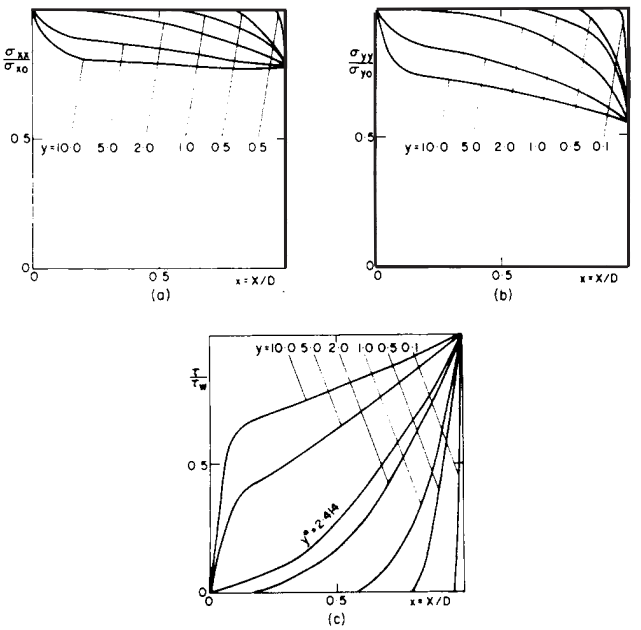

Fig. 3. Stress profiles at various cross sections of two-dimensional moving bed with one-dimensional flow ($\mu = 1.00$ and $\mu_w = 0.90$).

* The column and the flow are clearly symmetrical with respect to the y axis.

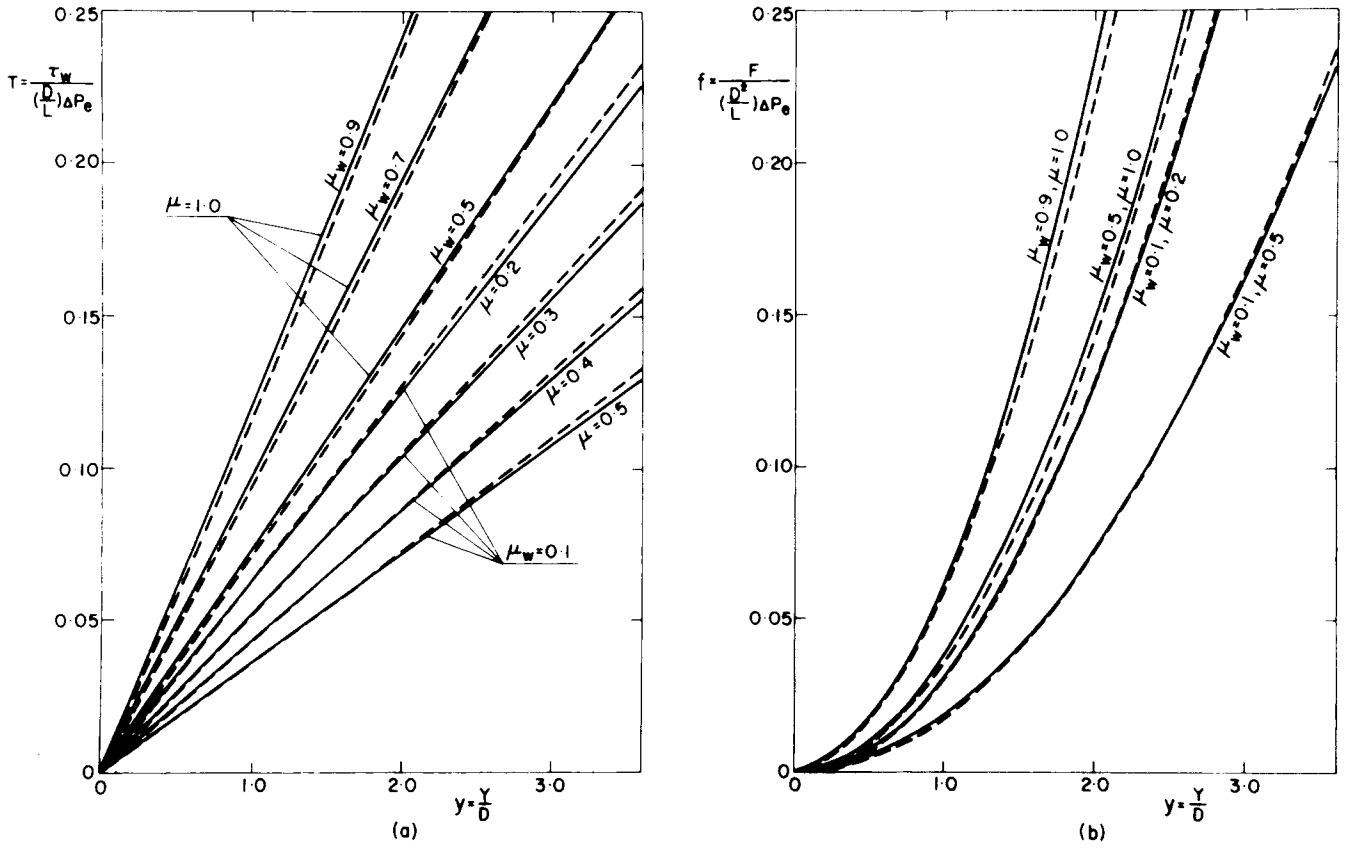

Fig. 4. Shear stress and total friction force at the wall of two-dimensional column with one-dimensional flow. Solid lines represent solution by method of characteristics; dotted lines represent solution by integral method.

defined by

$$f = \int_0^y T dy = \frac{1}{(D^2/L)\Delta P_e} \int_0^Y \tau_w dY = \frac{F}{(D^2/L)\Delta P_e} \tag{17}$$

While the driving force on the bed (supplied by the co-flow and gravity) increases linearly with y, the increase in f is stronger (Figure 4b) which means that at some point the driving force no longer exceeds friction. This sets an uper limit on the allowable length of the moving bed. An expression for this maximum length will be developed below.

Solution by Integral Method

Our main interest in the moving bed problem lies in the stresses and friction forces at the wall rather than in their detailed distribution within the bed. The solution of Equations (11), (12), and (8) may be considerably simplified by applying an integral method, which is most suitable for an analysis of this type and is often used, for example, in boundary layer theory. The method is based upon integrating the equilibrium equations with respect to x over the entire width of the bed, ending up with ordinary differential equations in y only which contain some integral expressions. The integrals are calculated by introducing an approximation for the stress distribution in the cross section of the bed. A good stress profile approximation requires some prior physical knowledge on the actual distribution and must satisfy the boundary conditions in x. The integral solution is then quite close to the exact one.

Our information on the boundary values of the stresses and their derivatives may be extended by combining Equations (8), (11), and (12) with the boundary conditions (9). At $x = 0$ we have*

$$\tau = 0; \quad \sigma_y = y; \quad \sigma_x = k_0 y \tag{18}$$

In a similar way we find for x = 1

$$\tau = T; \qquad \sigma_x = \frac{T}{\mu_w}$$

$$\sigma_y = \frac{T}{k_w \mu_w}; \quad \frac{\partial \tau}{\partial x} = 1 - \frac{1}{k_w \mu_w} \frac{dT}{dy} \tag{19}$$

where

$$k_0 = \frac{\sqrt{1+\mu^2} - \mu}{\sqrt{1+\mu^2} + \mu} = \frac{1 - \sin\delta}{1 + \sin\delta} \tag{20a}$$

$$k_w = \frac{1}{(\sqrt{1+\mu^2} + \sqrt{\mu^2 - \mu_w{}^2})^2 + \mu_w{}^2} = \frac{1 - \sin\delta \cos 2\psi_w}{1 + \sin\delta \cos 2\psi_w} \tag{20b}$$

By integrating Equations (11) and (12) and making use of (18) and (19), we obtain the integral equations

$$\frac{T}{\mu_w} + \frac{d}{dy}\left[\int_0^1 \tau dx\right] = k_0 y \tag{21}$$

$$\frac{d}{dy}\left[\int_0^1 \sigma_y dx\right] = 1 - T \tag{22}$$

* On the centerline of the column ($x = 0$) for $y < y^\circ$, $\frac{\partial \tau}{\partial x} = 0$. For $y > y^\circ$, $\frac{\partial \tau}{\partial x}$ is singular–positive toward the right and negative toward the left, with the same absolute value, by symmetry (see also Figure 3). By writing a force balance for a small element on the y axis, we can show, using symmetry arguments, that at $x = 0$ $\partial\sigma_y/\partial y = 1$ for all y, which is equivalent to setting $\frac{\partial \tau}{\partial x} = 0$ in Equation (12).

The solution begins by calculating the integral in Equation (21) choosing an approximate shear stress distribution of the form

$$\tau = Tx^q \tag{23}$$

which is similar in shape to the profiles shown in Figure 3c. q is given by

$$q = \frac{1}{T}\left(1 - \frac{1}{k_w\mu_w}\frac{dT}{dy}\right) \tag{24}$$

to satisfy the boundary conditions for τ in (18) and (19). Substituting (23) in (21) leads to the following equation for T:

$$\frac{T}{\mu_w} + \frac{d}{dy}\left[\frac{T^2}{1 + T - \frac{1}{k_w\mu_w}\frac{dT}{dy}}\right] = k_0 y \tag{25}$$

which may be solved numerically with the boundary condition $T = 0$ at $y = 0$. An analytical solution to this equation may be obtained for small y in the form of a power series:

$$T = \sum_{n=1}^{\infty} a_n y^n \tag{26}$$

where

$$a_1 = \mu_w \frac{\left(1 + \frac{k_0}{k_w}\right) - \sqrt{\left(1 - \frac{k_0}{k_w}\right)^2 + 8k_0\mu_w{}^2}}{2\left(\frac{1}{k_w} - 2\mu_w{}^2\right)} \tag{27a}$$

$$a_2 = a_1 \frac{(k_0\mu_w - a_1)}{2\left(\frac{1}{3} + \frac{k_0}{k_w}\right) + 4a_1\left(\mu_w - \frac{2}{3k_w\mu_w}\right)} \tag{27b}$$

and so on. Also, for large y there exists an asymptotic solution

$$T = k_0\mu_w(y - \mu_w) \tag{28}$$

The total friction force is obtained by integrating T with respect to y. For large y we have a good approximation

$$f = \frac{1}{2}k_0\mu_w y^2 \tag{29}$$

T and f from the integral solution are plotted in dotted lines in Figure 4 next to the results of the solution by the method of characteristics. The results of the two solutions are very close. The asymptotic solution indicates that T is directly proportional to μ_w and decreases with μ like k_0— the ratio of transverse to axial stress at the center.

We now return to Equation (22) where the integral represents the average dimensionless axial stress in a cross section of the bed and will be denoted by $\bar{\sigma}_y$. $\bar{\sigma}_y$ is found to be the difference between the dimensionless driving and friction forces:

$$\bar{\sigma}_y = y - f \tag{30}$$

A positive $\bar{\sigma}_y$ at the downstream end of the bed must be supported by the restraining screen (or by a similar device) to keep the bed in balance. $\bar{\sigma}_y = 0$ determines the maximum possible length of the moving bed. From (30) this length is found to be given approximately by

$$l_{\max} = \frac{2}{k_0\mu_w} \tag{31}$$

In the one-dimensional stress model of Janssen (1895), Delaplaine (1956), and Hancher and Jury (1959), the ratio k between the normal stress at the wall and the average axial stress was assumed to be constant. The wall stress T based on this model and expressed in terms of the variables used in the present study is given by

$$T = 1 - e^{-\mu_w k y}$$

It is easy to see that for small values of μ_w and k this result coincides with the asymptotic solution (28) of our present model where $k = k_0$. In other cases the two solutions deviate. Experiments by Brandt and Johnson (1963) have in fact shown that k is not quite a constant. From the results of the present analysis, k is found to be expressed by

$$k = \frac{\sigma_w}{\bar{\sigma}_y} = \frac{T}{\mu_w(y - f)} \tag{32}$$

AXISYMMETRICAL COLUMN WITH ONE-DIMENSIONAL FLOW

Figure 1a describing the two-dimensional column may also represent a cylindrical column with an axisymmetrical moving bed. The uniform one-dimensional flow at constant velocity v_0 results in $\partial P/\partial X = 0$, $\partial P/\partial Y = -\Delta P/L$, and equilibrium equations (6) and (7) become

$$\frac{\partial\sigma_x}{\partial x} + \frac{\sigma_x - \sigma_\theta}{x} + \frac{\partial\tau}{\partial y} = 0 \tag{33}$$

$$\frac{1}{x}\frac{\partial}{\partial x}(x\tau) + \frac{\partial\sigma_y}{\partial y} = 1 \tag{34}$$

with the extended boundary conditions (as in 3.2):

$$\left.\begin{aligned} &\text{at}\quad y = 0 \quad \sigma_x = \sigma_y = \tau = 0 \\ &\text{at}\quad x = 0 \quad \tau = 0;\quad \sigma_y = y;\qquad \sigma_x = k_0 y \\ &\text{at}\quad x = 1 \quad \tau = T;\quad \sigma_x = \frac{T}{\mu_w};\quad \sigma_y = \frac{T}{k_w\mu_w} \\ &\qquad\qquad \frac{\partial\tau}{\partial x} = 1 - T - \frac{1}{k_w\mu_w}\frac{dT}{dy} \end{aligned}\right\} \tag{35}$$

The circumferential stress σ_θ in Equation (33) may be expressed in terms of the other normal stresses through the Haar and Von Karman (1909) hypothesis. In the absence of shear stresses, σ_θ can be proved equal to σ_x, which is then a principal stress. The hypothesis states that when shear stresses are present, σ_θ is closely approximated by one of the principal stresses, in this case the one which approaches σ_x as the shear stresses tend to zero. The smaller the shear compared to the normal stresses, the closer σ_θ is to σ_x. It will be assumed in the present analysis that the shear stresses are indeed small compared to the normal ones, which is the case for friction coefficients small compared to unity, and therefore $\sigma_\theta \simeq \sigma_x$.

The integral method of solution will be adopted again here. Equations (33) and (34) integrated with respect to x from the center of the column to the wall yield, with the aid of (35), two integral equations similar to (21) and (22). The shear stress distribution given by (23) is chosen to calculate the integral in the first equation with q given the appropriate value to satisfy the conditions for τ in (35). The following equation is obtained for T:

$$\frac{T}{\mu_w} + \frac{\mathrm{d}}{dy}\left[\frac{T^2}{1 - \frac{1}{k_w\mu_w}\frac{dT}{dy}}\right] = k_0 y \tag{36}$$

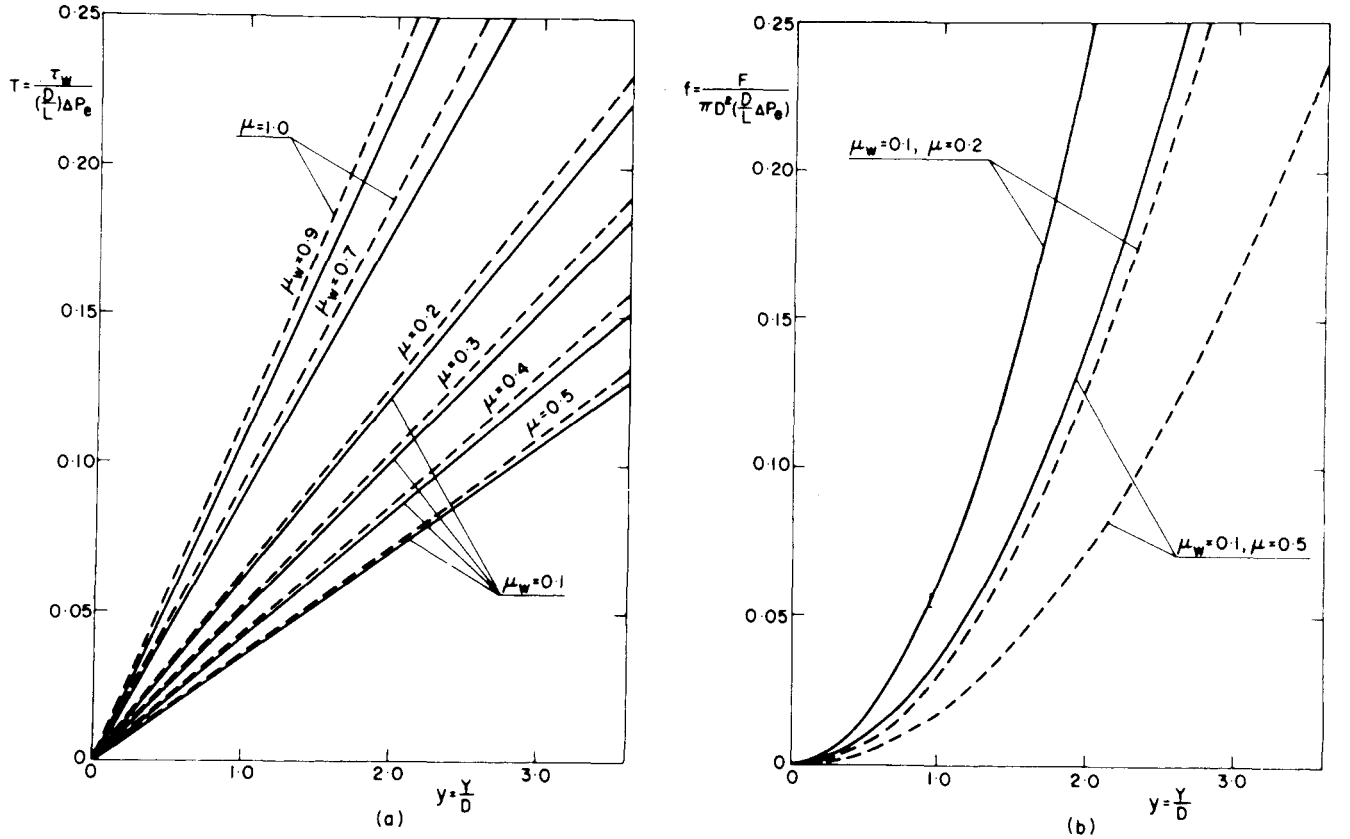

Fig. 5. Shear stress and total friction force at the wall of axisymmetrical column with one-dimensional flow. Same functions for two-dimensional geometry are shown in dotted lines for comparison.

with the boundary condition $T = 0$ at $y = 0$. (36) has an analytical solution in the form

$$T = Cy \tag{37}$$

where

$$C = \mu_w \frac{\left(1+\frac{k_0}{k_w}\right) - \sqrt{\left(1-\frac{k_0}{k_w}\right)^2 + 8k_0\mu_w^2}}{2\left(\frac{1}{k_w} - 2\mu_w^2\right)} \tag{38}$$

and the total friction force is therefore

$$f = \frac{1}{\pi}\int_0^y 2\pi T dy = Cy^2 \tag{39}$$

Figure 5 shows T and f as functions of y for different values of μ and μ_w. The results of the solution for the two-dimensional column are plotted along in dotted lines for comparison. Again, wall friction increases with μ_w and decreases with μ. The wall shear T is always lower for the axisymmetrical column than for the two-dimensional one. Note that $C = a_1$ where a_1 is the coefficient of the first power term in the series solution for small y, Equation (26) and (27). However, the total friction force is always higher in the axisymmetrical column than in the two-dimensional one, which may be explained by the fact that the former has more wall area per unit cross section area than the latter.

Let us compare again the results of the present analysis with the one-dimensional model of Janssen (1895), Delaplaine (1956), and Hancher and Jury (1959). There, the wall stress T for axisymmetrical geometry may be expressed by

$$T = 1 - e^{-2\mu_w k y}$$

which agrees well with (37) for small μ_w and k while $k = k_0$.

From the second integral equation, an expression similar to (30) is obtained for the average dimensionless axial stress. The maximum possible length of the moving bed is determined by $\bar{\sigma}_y = 0$

$$l_{\max} = \frac{1}{C} \tag{40}$$

and is always smaller than $l_{\max}$ for the two-dimensional geometry as given by (31).

Experimental data with axisymmetrical moving beds in a cylindrical column were obtained by Brandt and Johnson (1963). Their experimental apparatus consisted of a stationary, vertical bed of particles supported at the bottom by a screen attached to a balance, and of a column mounted on a rack which could be moved in both directions relative to the bed. The average axial stress was measured and plotted vs. bed depth. Unfortunately, a detailed comparison between the present theory and this data is not possible since no specific measurements were made to determine the friction coefficients μ and μ_w of the particles used. Values of those coefficients were deduced from the experimental results by fitting the data points to theoretical curves based on the one-dimensional model, as the bed was assumed to behave according to this model. As it turned out, the agreement with this model was not always good, especially in the case of counterflow. Qualitatively, the shape of the experimental curves of average axial stress vs. bed height fits the behavior obtained in the present model as described by Equation (30).

TWO-DIMENSIONAL COLUMN WITH AXIAL AND TRANSVERSE FLOW

Most of the moving bed systems designed to date have had screens in the column walls for fluid inlets and outlets (Aerhart et al., 1956; Hancher and Jury, 1959; Shwartz and Probstein, 1969; Gold et al., 1971, 1973). The fluid flow transverse to the bed motion in the vicinity

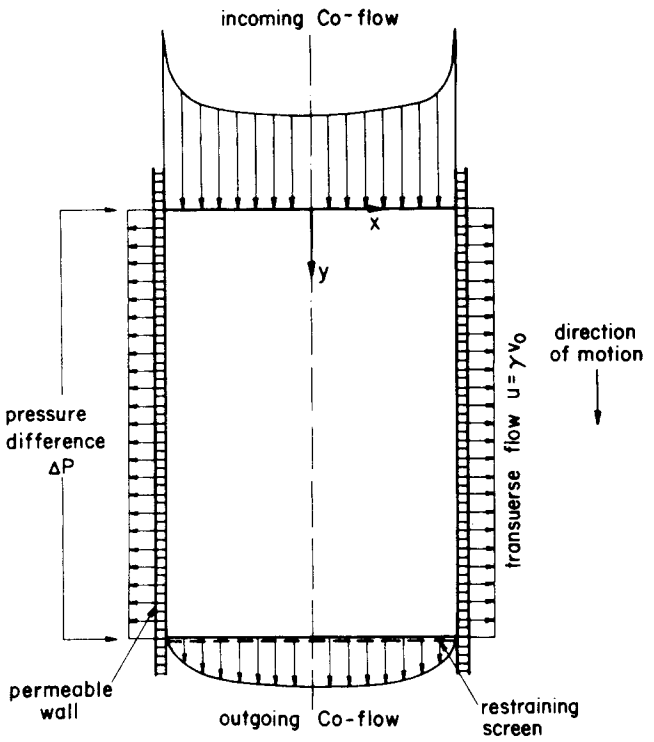

Fig. 6. Flow field in two-dimensional column with axial and transverse flow.

of the screens is associated with a pressure gradient from center to wall which has a marked effect on the wall stress. One goal of the present study which could not be achieved with earlier one-dimensional models (Janssen, 1895; Delaplaine, 1956; Hancher and Jury, 1959) has been to take this transverse flow into account and evaluate its effect.

Consider the two-dimensional column shown in Figure 6. It is similar in all aspects to the column dealt with before (Figure 1a) except that the impermeable wall is replaced by a porous one allowing a fraction of the main axial flow to penetrate through it. For simplicity of the analysis, it is assumed that the flow through the wall is uniform along its length at a velocity γv_0. The pressure difference between top and bottom of the bed remains ΔP as before. The effect of gravity on the bed motion is neglected.

The pressure and velocity distributions in the bed are governed by the equation of continuity and by Darcy's formula for flow through porous media, which can be combined into Laplace's equation for the pressure (Shwartz and Probstein, 1968). The equation may be solved for the present configuration with the appropriate boundary conditions to give the following pressure distribution:

$$p = (l - y) - \gamma p_1(x, y)$$

$$= (l - y) - \gamma \frac{4l}{\pi^2} \sum_{n=1}^{\infty} \frac{1}{(2n-1)^2} \frac{\cosh\left[(2n-1)\frac{\pi x}{l}\right] \sin\left[(2n-1)\frac{\pi y}{l}\right]}{\sinh\left[(2n-1)\frac{\pi}{l}\right]} \qquad (41)$$

from which the velocity field can be determined. The details of the solution are given in Appendix A. The pressure field is composed of a uniform gradient in the y direction as in the case of impermeable wall and of a secondary field p_1 due to the added transverse flow. Figure 6 describes the flow field in and out of the column showing the uniform velocity profile through the wall and the velocity distribution on the upstream and downstream ends. The flow field has two singular points on both ends of the bed at the wall, where the velocity reaches very high values due to the practically zero flow resistance of the fluid path from these points to the outside. The total incoming flow rate is higher by a factor of $(1 + \gamma l/2)$ than the one under the same pressure difference with impermeable wall. Likewise, the flow rate out the downstream end is lower by a factor of $(1 - \gamma l/2)$.

The dimensionless equilibrium equations for the column are (6) and (7) with the gravity term neglected, $m = 0$ and with p given by (41). The corresponding boundary conditions (9) may be extended with the aid of the Equations [as in (3.2)] to give

$$\text{at} \quad x = 0 \quad \tau = 0; \quad \sigma_x = k_0 \sigma_y = k_0[y - \gamma p_1(0, y)]$$

$$\text{at} \quad x = 1 \quad \tau = T; \quad \sigma_x = \frac{T}{\mu_w}; \quad \sigma_y = \frac{T}{k_w \mu_w} \qquad (42)$$

$$\frac{\partial \tau}{\partial x} = \left(1 - \frac{1}{k_w \mu_w} \frac{dT}{dy}\right) - \gamma \frac{\partial P_1}{\partial y}(1, y)$$

To apply the integral method of solution, Equations (6) and (7) are integrated with respect to x from center to wall and yield with the aid of (42):

$$\frac{T}{\mu_w} + \frac{d}{dy} \int_0^1 \tau dx = k_0 y + \gamma[(1 - k_0) p_1(0, y) - p_1(1, y)] \qquad (43)$$

$$\frac{d}{dy} \int_0^1 \sigma_y dx = 1 - T - \gamma \frac{d}{dy} \int_0^1 p_1 dx \qquad (44)$$

Once again a shear stress profile of the form described by (23) is chosen, with q given the appropriate value to satisfy the boundary conditions for τ in (42). By substituting the profile in (43) and evaluating the integral, the following equation is obtained for T:

$$\frac{T}{\mu_w} + \frac{d}{dy}\left[\frac{T^2}{1 + T - \frac{1}{k_w \mu_w}\frac{dT}{dy} - \gamma \frac{\partial p_1}{\partial y}(1, y)}\right] = k_0 y + \gamma[(1 - k_0) p_1(0, y) - p_1(1, y)] \qquad (45)$$

which can be solved numerically with the boundary condition $T = 0$ at $y = 0$.

Figure 7 describes the wall shear T and the total friction f as functions of y for different values of γ and l with fixed-bed properties. The dependence on y is similar to that with impermeable wall ($\gamma = 0$). There is a slight decrease of T with y for values of y close to l, due to the singularity of the flow field at this point. The effect of the transverse flow on the wall stress is clearly demonstrated by

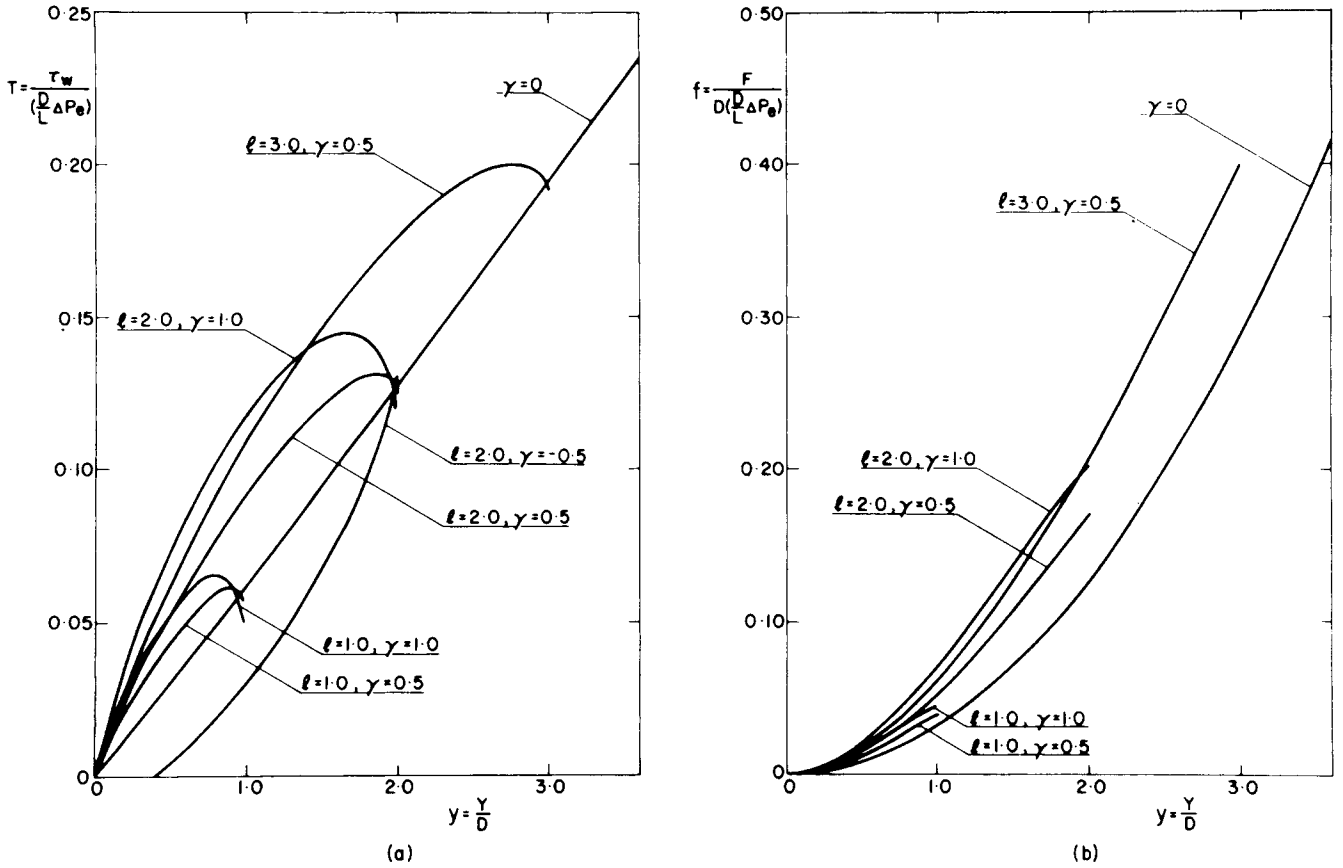

Fig. 7. Shear stress and total friction force at the wall of two-dimensional column with axial and transverse flow. Bed properties are $\mu = 0.20$, $\mu_w = 0.10$.

the increase of both T and f with γ and with l. It is interesting to note that for negative values of γ the wall stress is lower than that with impermeable wall. By reversing the flow through the wall and introducing fluid from the outside, a transverse pressure gradient from wall to center is formed, which opposes the transmission of axial forces sideways through the bed and reduces the stress normal to the wall and hence the friction.

The solution obtained for T from (45) may be substituted in the other integral Equation (44) to find the average axial stress and the maximum length of the bed.

NOTATION

a_n = constants in power series expansion of T, Equation (30)
C = constant defined by Equation (46)
c_1, c_2, c_3, c_4, c_n = constants of integration, Equations (A.8), (A.10)
D = half width or half diameter of the column
F = total friction force, Equation (21)
f = dimensionless total friction force, Equations (21), (47)
g = gravity
K = permeability of the bed
k = ratio between normal stress at the wall and average axial stress, Equation (37)
k_0 = dimensionless constant defined by Equation (24a)
k_w = dimensionless constant defined by Equation (24b)
L = length of the moving bed
l = dimensionless length of the moving bed, L/D
l_{max} = maximum length of the moving bed
n = integer index
P = fluid pressure
ΔP = pressure difference between the ends of the bed
ΔP_e = effective pressure difference between the ends of the bed, Equation (5)
p = dimensionless fluid pressure, Equation (6)
p_1 = secondary pressure field in column with permeable wall, Equation (50)
q = power of x in shear stress profile, Equation (27)
T = dimensionless shear stress at the wall
u = velocity component in the x direction
$\vec{V}$ = velocity vector
v = velocity component in the y direction
v_0 = fluid axial velocity in column with impermeable wall
X = transverse coordinate
x = dimensionless transverse coordinate, X/D
Y = axial coordinate
y = dimensionless axial coordinate, Y/D
y^* = the value of y corresponding to point B in Figure 3 where the wall effect has reached the center of the column

Greek Letters

γ = ratio of transverse velocity through permeable wall to the axial velocity with impermeable wall
δ = internal friction angle, $\tan^{-1}\mu$
δ_w = friction angle at the wall, $\tan^{-1}\mu_w$
ϵ = porosity of the bed
η = fluid viscosity
λ = constant, Equation (A.7)
μ = internal friction coefficient

μ_w = wall friction coefficient
ν = a function of y only in separation of variables of p_1, Equation (A.6)
ξ = a function of x only in separation of variables of p_1, Equation (A.6)
ρ_f = fluid density
ρ_s = density of solid particles in the bed
σ = mean normal stress (Figure 2)
σ_w = normal stress at the wall
σ_x = dimensionless normal stress in the transverse direction, Equation (6)
σ_{x0} = value of σ_{xx} at $x = 1$
σ_{xx} = normal stress in the transverse direction
σ_y = dimensionless normal stress in the axial direction, Equation (6)
σ_{y0} = value of σ_{yy} at $x = 0$
σ_{yy} = normal stress in the axial direction
$\bar{\sigma}_y$ = average axial stress, Equation (35)
σ_θ = dimensionless normal stress in the circumferential direction, Equation (11)
$\sigma_{\theta\theta}$ = normal stress in the circumferential direction
τ_w = shear stress at the wall
τ_{xy} = shear stress (cartesian coordinates)
ψ = angle with the principal axes, Figure 2
ψ_w = angle with the principal axes at the wall, Equation (20)

LITERATURE CITED

Aehart, T. A., J. C. Bresee, C. W. Hancher, and S. H. Jury, "Counter-current ion exchange," *Chem. Eng. Progr.*, **52**, 353 (1956).

Brandt, H. L., and B. M. Johnson, "Forces in a moving bed of particulate solids with interstitial fluid flow," *AIChE J.*, **9**, 771 (1963).

Delaplaine, J. W., "Forces acting in flowing beds of solids," *ibid.*, **2**, 127 (1956).

Gold, H., A. Todisco, G. Grossman, and A. A. Sonin, "Continuous moving bed ion exchange process," in *Proc. 32nd Ann. Meeting of the Intern. Water Conf.*, pp. 197-202, The Engineers Soc. of Western Penn., Pittsburgh (1971).

Gold, H., A. Todisco, A. A. Sonin, and R. F. Probstein, "The Avco continuous moving bed ion exchange process and large scale desalting," *Proc., 4th Intern. Symp. on Fresh Water from the Sea*, **3**, 57 (1973).

Haar, A., and T. von Karman, "Zur Theorie der Spannungszustande in plastischen und sandartigen Medien," *Nachrichten Ges. Wiss., Math.-Phys. Klasse*, Gottingen, Germany, 203-218 (1909).

Hancher, C. W., and S. H. Jury, "Semicontinuous countercurrent apparatus for contacting granular solids and solution," *Chem. Eng. Progr. Symp. Ser. No. 24*, **55**, 87 (1959).

Janssen, H. A., "Versuche Uber Getreidedruck in Silozellen," *Z. Verein Deutscher Ing.*, **39**, 1045 (1895).

Jenike, A. W., "Steady gravity flow of frictional cohesive solids in converging channels," *J. Appl. Mech.*, **31**, 5 (1964).

———., and J. R. Johanson, "On the theory of bin loads," *ASME Trans., J. Eng. Ind.*, **91**, 339 (1969).

———., "Review of the principles of flow of bulk solids," *CIM Trans.*, **73**, 141 (1970).

———., "Solids flow in bins and moving beds," *Chem. Eng. Progr.* **66**, 31 (1970).

Jenike, A. W., and R. T. Shield, "On the plastic flow of coulomb solids beyond original failure," *J. Appl. Mech.*, **27**, 599 (1959).

Johanson, J. R., "Stress and velocity fields in the gravity flow of bulk solids," *J. Appl. Mech.*, **86**, 499 (1964).

Sokolovski, V. V., *Statics of Granular Media*. Pergamon Press, London (1965).

Shwartz, J., and R. F. Probstein, "An analysis of counterwashers for freeze-distillation desalination," *Desalination*, **4**, 5 (1968).

———., "Experimental study of slurry separators for use in desalination," *ibid.*, **6**, 239 (1969).

APPENDIX A. PRESSURE AND VELOCITY DISTRIBUTION IN A TWO-DIMENSIONAL MOVING BED WITH AXIAL AND TRANSVERSE FLOW

The pressure and velocity distributions in the bed (Figure 6) are governed by the equation of continuity

$$\nabla \cdot \vec{V} = \frac{\partial u}{\partial X} + \frac{\partial v}{\partial Y} = 0 \tag{A.1}$$

and by Darcy's formula for flow through porous media:

$$u = -\frac{K}{\eta}\frac{\partial P}{\partial X}; \quad v = -\frac{K}{\eta}\frac{\partial P}{\partial Y} \tag{A.2}$$

(A.1) and (A.2) can be combined into a Laplace equation for the pressure which may be written in a dimensionless form using (5):

$$\frac{\partial^2 p}{\partial x^2} + \frac{\partial^2 p}{\partial y^2} = 0 \tag{A.3}$$

with the boundary conditions:

$$\text{at } x = 0 \quad \frac{\partial p}{\partial x} = 0 \qquad \text{(symmetry)} \tag{A.4a}$$

$$\text{at } x = 1 \quad \frac{\partial p}{\partial x} = -\gamma \qquad \text{(uniform velocity through the wall)} \tag{A.4b}$$

$$\left.\begin{array}{ll} \text{at } y = 0 & p = l \\ \text{at } y = l & p = 0 \end{array}\right\} \quad \text{(pressure difference } \Delta P \text{ between top and bottom of the bed)} \tag{A.4c, A.4d}$$

To solve for p, let

$$p = (l - y) + \gamma p_1(x, y) \tag{A.5}$$

Here p_1 has to satisfy Laplace's equation and the same boundary conditions (A.4) as p, except that at $y = 0$, $p^1 = 0$ and at $x = 1$ $\partial p_1/\partial x = -1$. Applying separation of variables:

$$p_1(x, y) = \xi(x)\nu(y) \tag{A.6}$$

hence, from (A.3)

$$\frac{\xi''}{\xi} = -\frac{\nu''}{\nu} = \lambda^2 \tag{A.7}$$

where λ is a constant. Solving for ξ and ν we have

$$p_1 = \xi\nu = (c_1 \cosh \lambda x + c_2 \sinh \lambda x)(c_3 \cos \lambda y + c_4 \sin \lambda y) \tag{A.8}$$

where c_1, c_2, c_3, and c_4 are constants of integration. By applying the boundary conditions (A.4a), (A.4c), and (A.4d), c_2, c_3, and λ are determined and (A.8) reduces to the form

$$p_1 = c_1 c_4 \cosh\left(\frac{n\pi x}{l}\right)\sin\left(\frac{n\pi y}{l}\right) \tag{A.9}$$

where n is any integer. Since the equation is linear, p_1 may be rewritten as a sum of terms like in (A.9) for all values of n, replacing the product c_1c_4 by constants c_n:

$$p_1 = \sum_{n=1}^{\infty} c_n \cosh\left(\frac{n\pi x}{l}\right)\sin\left(\frac{n\pi y}{l}\right) \tag{A.10}$$

By differentiating (A.10) with respect to x, the pressure gradient at the wall is obtained in the form of a Fourier series in y. The constants c_n are determined by applying the last boundary condition (A.4b):

$$c_n = \frac{2l}{(n\pi)^2}\,\frac{[(-1)^n - 1]}{\sinh\left(\frac{n\pi}{l}\right)} \tag{A.11}$$

and, therefore,

$$p = (l - y) - \gamma \frac{4l}{\pi^2} \sum_{n=1}^{\infty} \frac{1}{(2n-1)^2} \frac{\cosh\left[\frac{(2n-1)\pi x}{l}\right] \sin\left[\frac{(2n-1)\pi y}{l}\right]}{\sinh\left[\frac{(2n-1)\pi}{l}\right]} \tag{41}$$

The velocity field may be obtained from (41) by Darcy's formula (A.2):

$$\frac{u}{v_0} = \gamma \frac{4}{\pi} \sum_{n=1}^{\infty} \frac{1}{(2n-1)} \frac{\sinh\left[\frac{(2n-1)\pi x}{l}\right]}{\sinh\left[\frac{(2n-1)\pi}{l}\right]} \sinh\left[\frac{(2n-1)\pi y}{l}\right] \tag{A.12}$$

$$\frac{v}{v_0} = 1 + \gamma \frac{4}{\pi} \sum_{n=1}^{\infty} \frac{1}{(2n-1)} \frac{\cosh\left[\frac{(2n-1)\pi x}{l}\right] \cos\left[\frac{(2n-1)\pi y}{l}\right]}{\sin\left[\frac{(2n-1)\pi}{l}\right]} \tag{A.13}$$

The total incoming and outgoing flow rates at the ends of the bed may be found by integrating v in (A.13) with respect to x from one wall to the other for $y = 0$ and $y = l$, respectively.

Manuscript received October 23, 1974, revision received February 14 and accepted February 17, 1975.

Hydrogenation of Acetone in a Vibrating Slurry Reactor

The behavior of a vibrating column of liquid as a slurry reactor and the dependence of the mass transfer resistances on the frequency of oscillation and liquid temperature were studied. The hydrogenation of liquid acetone over Raney nickel was chosen as the model reaction. The tortuosity factor of the catalyst was determined from measurements with two different particle sizes.

N. O. LEMCOFF and G. J. JAMESON

Department of Chemical Engineering Imperial College, London, SW7, England

SCOPE

Slurry reactors are used in the chemical industry in processes involving heterogeneous catalysis where a gas reacts with a liquid on a solid catalyst. They are mainly used in small-scale batch reactions and in hydrogenations.

When stirred tanks are used as slurry reactors, diffusional limitations are found quite often. The hydrogenation of α-methylstyrene on supported and black palladium was investigated in different slurry reactors (Johnson, et al., 1957; Sherwood and Farkas, 1966) and the mass transfer to the solid catalyst was the rate determining step. The same effect was found in the hydrogenation of nitrobenzene over palladium (Snyder et al., 1957) and of cyclohexene over platinum and palladium (Price and Schiewetz, 1957; Sherwood and Farkas, 1966).

Since mass transfer is generally the limiting factor, an improvement in the agitation will increase the yield of the reaction. Several authors have reported that when a column of liquid is made to oscillate vertically, a considerable increase in the gas-liquid (Buchanan et al., 1963; Jameson, 1966) and solid-liquid (Lemcoff and Jameson, 1975) mass transfer rates is obtained. When the oscillation frequency is greater than a certain limit, a cycling of bubbles is produced which generates very high turbulence and interfacial areas (Jameson, 1966), contributing to the above mentioned effect (resonant bubble contactor).

The purpose of this work is to use this vibrating contactor in the hydrogenation of aqueous acetone on Raney nickel and to analyze the effect of the bubble cycling on the diffusional resistances, with a view to using this contactor for solid catalyzed gas-liquid reactions in general. The rate of hydrogenation is determined at constant pressure from volumetric measurements, and the effect the temperature, pressure, oscillation frequency, and bubble cycling have on it is studied. At the same time, the pore diffusion in the catalyst particle is analyzed and its tortuosity factor is determined.

CONCLUSIONS AND SIGNIFICANCE

The tortuosity factor of the Raney nickel catalyst was 4.0, in agreement with published results for similar catalysts (Satterfield, 1970). The apparent activation energies for the hydrogenation of acetone, determined in the absence of external diffusional effects, were 10.1 for Nicat 102 and 5.7 kcal/gmole for Nicat 820. The smallest catalyst particle had an effectiveness factor of one, while the largest operated in the asymptotic zone, and therefore the first value quoted is that associated with the rate of reaction constant.

Solid-liquid and gas-liquid diffusional effects become negligible at frequencies of oscillation above 1500 rev./

N. O. Lemcoff is with the Centro de Investigación y Desarrollo en Procesos Catalíticos (CINDECA), Facultad de Ciencias Exactas, 47 y 115, La Plata, Argentina.